Structural Consequences of Hydrophilic Amino Acid Substitutions in the Hydrophobic Pocket of Human Carbonic Anhydrase II†

Satish K. Nair and David W. Christianson*

Department of Chemistry, University of Pennsylvania, Philadelphia, Pennsylvania 19104-6323

Received November 25, 1992; Revised Manuscript Received February 2, 1993

ABSTRACT: The three-dimensional structures of Leu-198→Glu, Leu-198→His, Leu-198→Arg, and Leu-198→Ala variants of human carbonic anhydrase II (CAII) have each been determined by X-ray crystallographic methods to a resolution of 2.0 Å. The side chain of Leu-198 is located at the mouth of the active site hydrophobic pocket, and this pocket is required for substrate association. Hydrophobic → hydrophilic amino acid substitutions at the mouth of the pocket decrease k_{cat}/K_M for CO_2 hydration: the CO_2 hydrase activities of Leu-198→Glu, Leu-198→His, and Leu-198→Arg CAIIs are diminished 19-fold, 10-fold, and 17-fold, respectively, relative to the wild-type enzyme; however, the substitution of a compact aliphatic side chain for Leu-198 has a smaller effect on catalysis, in that Leu-198→Ala CAII exhibits only a 3-fold decrease in CO_2 hydrase activity [Krebs, J. F., Rana, F., Dluhy, R. A., & Fierke, C. A. (1993) *Biochemistry* (preceding paper in this issue)]. It is intriguing that CO_2 hydrase activity is not severely diminished in Leu-198→Arg CAII, even though the side chain of Arg-198 blocks the hydrophobic pocket. Therefore, the bulky side chain of Arg-198 must be reasonably mobile in order to accommodate substrate association. Significantly, a residue larger than the wild-type Leu-198 side chain does not necessarily block the substrate association pocket; e.g., the side chain of Glu-198 packs against a hydrophobic patch, the net result of which is a wider mouth for the pocket. The so-called "deep" water molecule, which resides at the mouth of the hydrophobic pocket in a location believed to be the precatalytic association site for substrate, is not displaced in any of the variants. Since the structure of the CO_2 association site is not severely compromised, it is reasonable that catalytic efficiency is not severely compromised in Leu-198 variants. Finally, the effects of residue 198 on structure–activity relationships of nucleophilic zinc-bound hydroxide are minimal, except in the Leu-198→Glu variant.

The carbonic anhydrases are prototypical zinc metalloenzymes for which the only known biological function is the catalytic hydration of carbon dioxide to form bicarbonate ion and acid (H^+). In the human erythrocyte, isozyme II (CAII;[1] EC 4.2.1.1) catalyzes the CO_2 hydration reaction with kinetics approaching that of a diffusion-controlled process: $k_{cat}/K_M = 1.5 \times 10^8\ M^{-1}\ s^{-1}$ [for recent reviews, see Coleman (1986), Lindskog (1986), Silverman and Lindskog (1988), and Christianson (1991)]. Since catalytic turnover requires the transfer of the proton product to bulk solvent, for which the upper limit is typically $10^3\ s^{-1}$ (Eigen & Hammes, 1963), an excess of buffer is required to accept this proton in order to achieve the measured turnover rate of $10^6\ s^{-1}$ (Silverman & Tu, 1975; Jonsson et al., 1976).

The structure of carbonic anhydrase II from human blood has been determined (Liljas et al., 1972) and refined (Eriksson et al., 1986, 1988) at 2.0-Å resolution. The active site of the enzyme is a cone-shaped cleft about 15 Å deep. The imidazole side chains of His-94, His-96, and His-119 coordinate to zinc at the base of this cleft, and hydroxide ion completes the tetrahedral metal coordination polyhedron; importantly, zinc-bound hydroxide is the catalytically active nucleophile (Coleman, 1967; Lindskog & Coleman, 1973). Important polar residues in the active site include Thr-199, which accepts a hydrogen bond from zinc-bound hydroxide and donates a hydrogen bond to Glu-106 (Eriksson et al., 1986, 1988), and His-64, which serves as a proton shuttle in the conversion of zinc-bound water into zinc-bound hydroxide (Steiner et al., 1975; Tu et al., 1989).

A hydrophobic pocket is adjacent to zinc-bound hydroxide in the CAII active site, and the so-called "deep" water molecule resides at the mouth of this pocket and makes van der Waals contacts with the side chains of Leu-198 and Trp-209 (Lindskog, 1986; Eriksson et al., 1986, 1988). These two enzyme residues, along with Val-121, constitute the mouth of the hydrophobic pocket. Residue Val-143 comprises the base of the pocket, and recent genetic–structural studies focus on the structural and functional importance of this residue (Fierke et al., 1991; Alexander et al., 1991) as well as Val-121 (Nair et al., 1991). These studies provide the first proof that the hydrophobic pocket is required for substrate association, although a unique precatalytic substrate binding mode is not a prerequisite for efficient catalysis.

The current genetic–structural analysis of the hydrophobic pocket centers on hydrophobic → hydrophilic amino acid substitutions at residue Leu-198. The three-dimensional structures of enzyme variants Leu-198→Glu (L198E), Leu-198→His (L198H), and Leu-198→Arg (L198R) have each been determined by X-ray crystallographic methods to a limiting resolution of 2.0 Å. Additionally, the structure of Leu-198→Ala (L198A) CAII has been determined at 2.0-Å resolution, and the structural consequences of this conservative nonpolar → nonpolar substitution are contrasted with those assessed for the radical nonpolar → polar substitutions. Furthermore, Leu-198 CAII variants exhibit substantial differences in CO_2 hydration kinetics: the relative losses of CO_2 hydrase activity measured for L198E, L198H, L198R, and L198A CAIIs at pH 8.9 are 19-fold, 10-fold, 17-fold, and

† We thank the NIH for Grant GM45614. D.W.C. is an Alfred P. Sloan Research Fellow, and S.K.N. is supported in part by NIH Training Grant GM07229.

[1] Abbreviations: CAII, human carbonic anhydrase II; CAIII, human carbonic anhydrase III; L198E, Leu-198→Glu; L198H, Leu-198→His; L198R, Leu-198→Arg; L198A, Leu-198→Ala.

0006-2960/93/0432-4506$04.00/0

3-fold, respectively (Krebs et al., 1993). Here, these kinetic results are interpreted in light of three-dimensional protein structures, and this powerful genetic–structural approach delineates the contribution of Leu-198 to substrate association and catalysis.

EXPERIMENTAL PROCEDURES

Recombinant L198E, L198R, L198H, and L198A CAIIs were generously provided by Prof. Carol Fierke, Duke University, and enzyme crystallizations were performed by the sitting-drop method. Typically, a 5-μL drop containing 0.3 mM enzyme, 50 mM Tris-HCl (pH 8.0 at room temperature), and 3 mM NaN_3 was added to a 5-μL drop of precipitant buffer containing 50 mM Tris-HCl (pH 8.0 at room temperature) and 3 mM NaN_3 with 1.75–2.5 M ammonium sulfate; the surrounding crystallization well was additionally charged with 1 mL of precipitant buffer. Both solutions were saturated with methylmercury acetate in order to facilitate the growth of diffraction-quality parallelepipeds. The addition of 0.5 mM hexyl β-glucoside to the enzyme buffer was critical for the crystallization of L198E CAII, and crystals of L198H and L198A CAIIs did not contain azide. Additionally, the structures of azide-free L198E and L198R CAIIs are identical to those reported here, which were determined in the presence of azide (Nair and Christianson, unpublished results). For L198H CAII, addition of mercurymethyl acetate resulted in immediate protein precipitation; however, crystals grown in the absence of mercury exhibited suitable diffraction properties, and these were used for X-ray data collection. Crystals of each variant achieved typical dimensions of 0.2 mm × 0.2 mm × 0.8 mm within 2 weeks at 4 °C; these crystals, like those obtained from the wild-type enzyme (Eriksson et al., 1986, 1988; Alexander et al., 1991), belong to space group $P2_1$ with unit cell parameters of a = 42.7 Å, b = 41.7 Å, c = 73.0 Å, and β = 104.6°.

Protein crystals were mounted and sealed in 0.5-mm glass capillaries with a small portion of mother liquor. X-ray diffraction data were measured at room temperature on a Siemens X-100A multiwire area detector, mounted on a three-axis camera and equipped with Charles Supper double X-ray focusing mirrors; Cu Kα radiation was supplied by a Rigaku RU-200 rotating anode operating at 45 kV/50 mA. The crystal-to-detector distance was set at 10 cm, and the detector swing angle was fixed at 22° in a minimum of two data acquisition runs per experiment. Data frames of 0.083° oscillation about ω were collected, with exposure times of 60 s/frame, for total angular rotation ranges about ω of at least 70° per run. Multiple data sets were collected from each crystal, and diffraction intensities were measured to a limiting resolution of 2.0 Å. Raw data frames were processed using the BUDDHA package (Durbin et al., 1986), and intensity data were corrected for Lorentz and polarization effects. Replicate and symmetry-related structure factors were merged using PROTEIN (Steigemann, 1974); relevant data reduction statistics are recorded in Table I.

Structure factors obtained from corrected intensity data were used to generate difference electron density maps using Fourier coefficients $(2|F_o|-|F_c|)$ and $(|F_o|-|F_c|)$ with calculated structure factors and phases derived from the structure of wild-type CAII, less the atoms of Leu-198 and active site solvent molecules. All model building was done with the graphics software FRODO (Jones, 1985) installed on an Evans and Sutherland PS390 interfaced with a VAXstation 3500. Inspection of the initial electron density maps revealed that only minor adjustments to the protein models were required, although subtle differences in active site solvent structure among the four CAII mutants were noted at this stage.

Table I: Data Collection and Refinement Statistics for CAII Variants

	L198E	L198H	L198R	L198A
no. of crystals	1	1	1	1
no. of measured reflections	17 655	21 384	24 605	25 456
no. of unique reflections	13 289	12 138	13 615	13 017
max resolution (Å)	2.0	2.0	2.0	2.0
R_{merge}[a]	0.058	0.066	0.078	0.078
no. of water molecules in final cycle of refinement	107	91	110	107
no. of reflections used in refinement	12 137	10 938	12 421	12 248
completeness of data (%)	76	69	78	77
R factor[b]	0.180	0.182	0.182	0.186
rms deviation from ideal bond lengths (Å)	0.016	0.015	0.011	0.014
rms deviation from ideal bond angles (deg)	1.0	1.1	2.3	1.1
rms deviation from ideal planarity (Å)	0.011	0.010	0.012	0.010
rms deviation from ideal chirality (Å^3)	0.103	0.090	0.102	0.100

[a] R_{merge} for replicate reflections: $R = \sum|I_{hi} - \langle I_h\rangle|/\sum\langle I_h\rangle$; I_{hi} = intensity measured for reflection h in data set i; $\langle I_h\rangle$ = average intensity calculated for reflection h from replicate data. [b] Crystallographic R factor: $R = \sum||F_o| - |F_c||/\sum|F_o|$; $|F_o|$ and $|F_c|$ are the observed and calculated structure factors, respectively.

The atomic coordinates of each CAII mutant were refined against the observed data using PROLSQ (Hendrickson & Konnert, 1981; Hendrickson, 1985). When the crystallographic R factor dropped below 0.20, the variant side chain of residue 198 and active site solvent molecules were built into difference electron density maps calculated with structure factors and phases derived from the in-progress atomic model. During subsequent rounds of refinement, solvent molecules were routinely examined and deleted if their thermal B factors exceeded 50 Å^2. For each CAII variant, refinement converged smoothly to a final R factor within the range 0.180–0.186. Each final model had excellent stereochemistry with rms deviations from ideal bond lengths and angles within the ranges 0.011–0.016 Å and 1.0–2.3°, respectively. Pertinent refinement statistics are recorded in Table I.

For each of the refined structures, a difference electron density map calculated with Fourier coefficients $(|F_o| - |F_c|)$ and phases derived from the coordinates of each final model revealed that the highest peaks in the vicinity of the active site were just under 3.5σ in each structure. The rms error in atomic positions for each structure was estimated to be ca. 0.25 Å on the basis of relationships derived by Luzzati (1952). The coordinates of each mutant CAII have been submitted to the Brookhaven Protein Data Bank (Bernstein et al., 1977), with reference codes as follows: L198E CAII, 1HEB; L198R CAII, 1HEA; L198H CAII, 1HEC; L198A CAII, 1HED.

RESULTS

Apart from the contour of the hydrophobic surface flanking residue 198, the refined structures of CAII variants at this position do not differ substantially from the structure of the wild-type enzyme. However, we note that unambiguous electron density for His-4 is observed in maps of L198R and L198A CAIIs, whereas this residue was not registered in the structure of wild-type CAII due to a lack of interpretable electron density. Other differences include the conformations of occasional surface residues, but this is most likely the result of weak electron density often observed for mobile residues

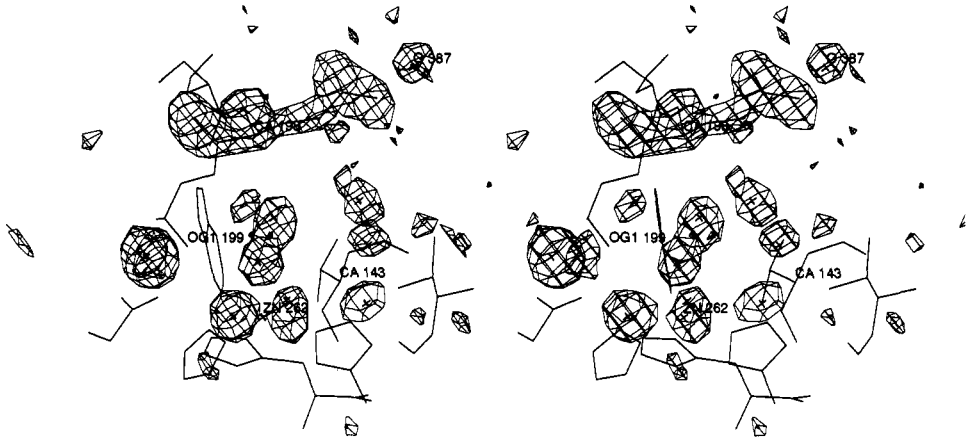

FIGURE 1: Difference electron density map of L198E CAII, calculated with Fourier coefficients ($|F_o| - |F_c|$) and phases calculated from the final model less the atoms of Glu-198 and active site solvent molecules. Refined atomic coordinates are superimposed on the map (contoured at 2.5σ); Glu-198, Thr-199, Val-143, and zinc are indicated. The carboxylic acid side chain of Glu-198 packs against the hydrophobic wall of the active site and does not block the pocket; the deep water molecule (Lindskog, 1986) remains in place at the mouth of the hydrophobic pocket. Note that the carboxylic acid of Glu-198 engages a solvent molecule (HOH 387 or, alternately, an ammonium counterion) in a syn-oriented hydrogen bond.

on the surface of the protein. Finally, there are subtle changes in the active-site solvent structure which accompany each mutation at residue 198. In this section, we describe the specific structural features characterizing the hydrophobic pocket of each mutant CAII, and we then summarize the differences observed in the zinc coordination polyhedra among the mutants.

Unexpectedly, the three-dimensional structure of L198E CAII reveals that the polar side chain of Glu-198 packs against the flanking hydrophobic surface defined by active site residues Pro-202, Phe-131, Leu-141, and Leu-204. In effect, the mouth of the hydrophobic pocket is *wider* in this mutant, even though the mutant side chain is larger than that of the wild-type enzyme (an electron density map is found in Figure 1). Accordingly, it is not surprising that the pK_a of Glu-198 is elevated to either ca. 5.9 or 8.9 [it is not certain which of the two activity-linked pK_a values corresponds to Glu-198; see Kreb et al. (1993)]. Given that no structural changes are observed for Glu-198 in an X-ray crystallographic investigation conducted at pH 10.0, it could be inferred that the pK_a of Glu-198 is 5.9 *if* a structural change were expected to accompany its ionization (Nair and Christianson, unpublished results). We note that an active site water molecule (HOH 387 in wild-type CAII) appears to move 1.5 Å from its position in the wild-type enzyme in order to hydrogen bond to Glu-198 with favorable *syn*-bidentate stereochemistry. Additionally, the so-called deep water moves 2.9 Å across the mouth of the hydrophobic pocket to occupy a position closer to that observed for the deep water in the native blood enzyme (Eriksson 1986, 1988).

Significant conformational changes are observed for the carboxylic acid side chain of Glu-198 relative to the aliphatic side chain of Leu-198 in the wild-type enzyme. The side-chain torsion angles of Leu-198 ($\chi_1 = -71°$ and $\chi_2 = 179°$) are in agreement with the distribution of preferred values determined by Ponder and Richards (1987) in an analysis of refined protein structures. However, although side-chain torsion angles χ_1 and χ_3 of Glu-198 are close to optimal values, torsion angle χ_2 deviates from optimal values (Table II; Ponder & Richards, 1987). It is reasonable that the side chain of Glu-198 sacrifices optimal torsion angle values in order to optimize its van der Waals contact surface area with the hydrophobic wall flanking this residue. Finally, the least-squares superposition of wild-type and L198E CAIIs yields an rms deviation of 0.14 Å for Cα atoms between the two structures.

Table II: Residue 198 Torsion Angles in CAII Variants (deg)

	wild type	L198E	L198H	L198R	L198A
ϕ	−73	−66	−70	−73	−71
ψ	+155	+156	+159	+156	+153
χ_1	−71	−72	−62	−67	
χ_2	+179	+152	−23	−179	
χ_3		−18		+101	
χ_4				−68	

The three-dimensional structure of L198H CAII reveals that the imidazole group of His-198 packs against its flanking hydrophobic wall, in a manner similar to that observed for the side chain of Glu-198. A wider mouth to the hydrophobic pocket results (an electron density map is found in Figure 2, and a superposition of L198E and L198H CAIIs is found in Figure 3). Given that L198H CAII was crystallized in the absence of Hg^{2+}, it is not surprising that the side chain of Cys-206 is directed toward the active site in a conformation similar to that observed in the Hg^{2+}-free native blood enzyme (in the presence of Hg^{2+}, this side chain points away from the active site in order to ligate the metal ion). We note that the sulfur atom of Cys-206 is within hydrogen-bonding distance (3.4 Å) to the Nε atom of His-198, but this interaction is characterized by unfavorable hydrogen bond stereochemistry to histidine.

The torsion angles of His-198 are reported in Table II. As in L198E CAII, torsion angle χ_2 deviates from optimal values (Ponder & Richards, 1987) as a result of optimized van der Waals contact between the imidazole side chain and the flanking hydrophobic region. The rms deviation of Cα atoms between L198H CAII and the wild-type enzyme is 0.15 Å.

In contrast with L198E and L198H CAIIs, the three-dimensional structure of L198R CAII reveals that the mutant side chain protrudes into the active site and partially blocks the hydrophobic pocket. Here, the mouth of the hydrophobic pocket is substantially narrower, as would be expected by the substitution of a side chain larger than leucine at position 198 (an electron density map is found in Figure 4). Consequently, an active site water molecule (HOH 381 in the wild-type structure) is displaced by Arg-198, although this is not the so-called deep water molecule presumably displaced by

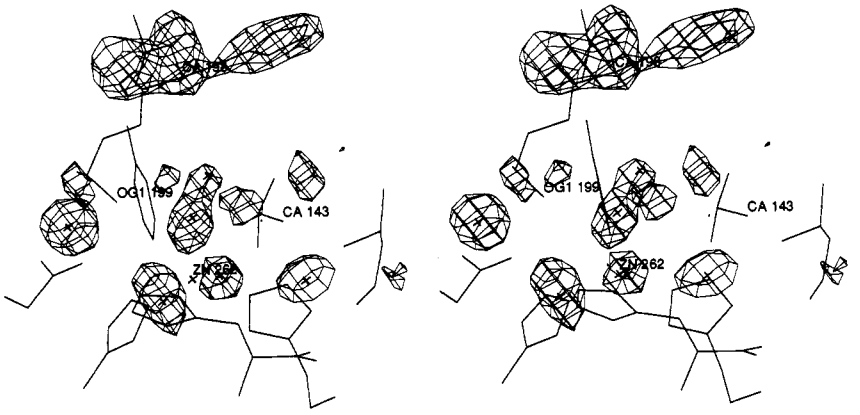

FIGURE 2: Difference electron density map of L198H CAII, calculated with Fourier coefficients ($|F_o| - |F_c|$) and phases calculated from the final model less the atoms of His-198 and active site solvent molecules. Refined atomic coordinates are superimposed on the map (contoured at 2.5σ); His-198, Thr-199, Val-143, and zinc are indicated. The imidazole side chain of His-198 packs against the hydrophobic wall of the active site and does not block the pocket; the deep water molecule (Lindskog, 1986) remains in place at the mouth of the hydrophobic pocket.

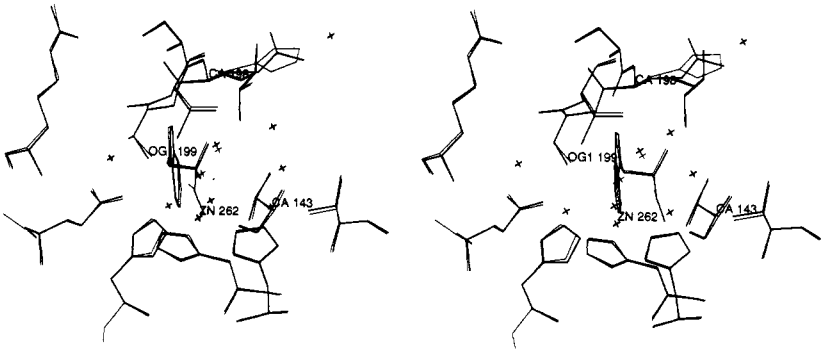

FIGURE 3: Superposition of L198E CAII (thick bonds) and L198H CAII (thin bonds). Enzyme residues Val-143, Thr-199, residue 198, and the active site zinc ion are indicated. The polar side chains of Glu-198 and His-198 each pack in a similar manner against the hydrophobic wall of the active site, which results in a wider mouth for the hydrophobic pocket.

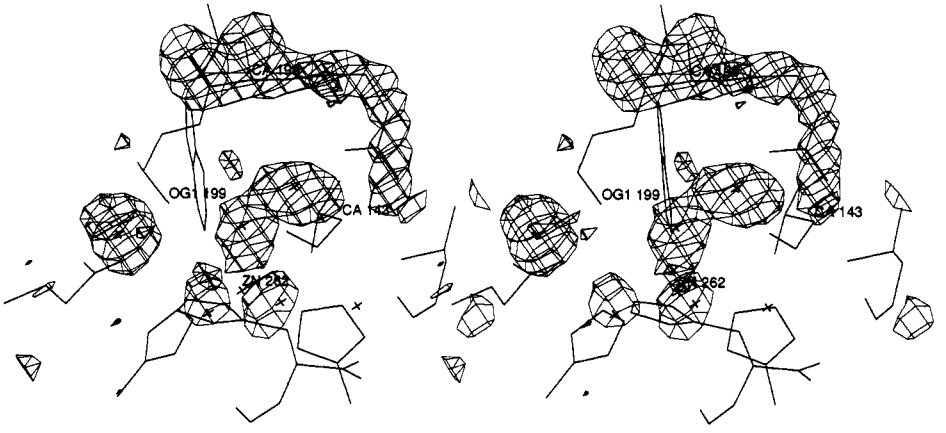

FIGURE 4: Difference electron density map of L198R CAII, calculated with Fourier coefficients ($|F_o| - |F_c|$) and phases calculated from the final model less the atoms of Arg-198 and active site solvent molecules. The map is contoured at 2.5σ, and refined atomic coordinates are superimposed; Arg-198, Thr-199, Val-143, and zinc are indicated. Although the side chain appears to block the mouth of the hydrophobic pocket, it does not make any hydrogen bond interactions with the protein. We suspect that Arg-198 is sufficiently mobile such that CO_2 association with the hydrophobic pocket is not too severely hindered. The lack of bifurcated electron density for the guanidinium group of Arg-198 could be consistent with the interpretation of mobility for this residue.

substrate association (Lindskog, 1986; Eriksson, 1986, 1988). The deep water molecule remains at the mouth of the pocket in a position 1.8 Å away from its position observed in the wild-type enzyme, and its closest contact to Arg-198 is 3.6 Å (with NH1).

The substitution of the large guanidinium side chain at residue 198 does not alter the backbone conformation of residue 198 as compared with the wild-type enzyme, and amino acid torsion angles are reported in Table II. Additionally, although the side-chain torsion angle χ_3 of Arg-198 tends toward an eclipsed conformation, torsion angles χ_1, χ_2, and χ_4 are close to optimal trans and gauche values determined in analyses of experimentally determined protein structures (Janin et al., 1978; Bhat et al., 1979). A least-squares superposition of wild-type and L198R CAIIs is found in Figure 5; the rms deviation of Cα atoms is 0.16 Å between the two structures. For comparison, the coordinates of L198E CAII are additionally superimposed on the structures found in Figure 5.

We note that the closest contact between the positively charged zinc ion and the positively charged guanidinium group

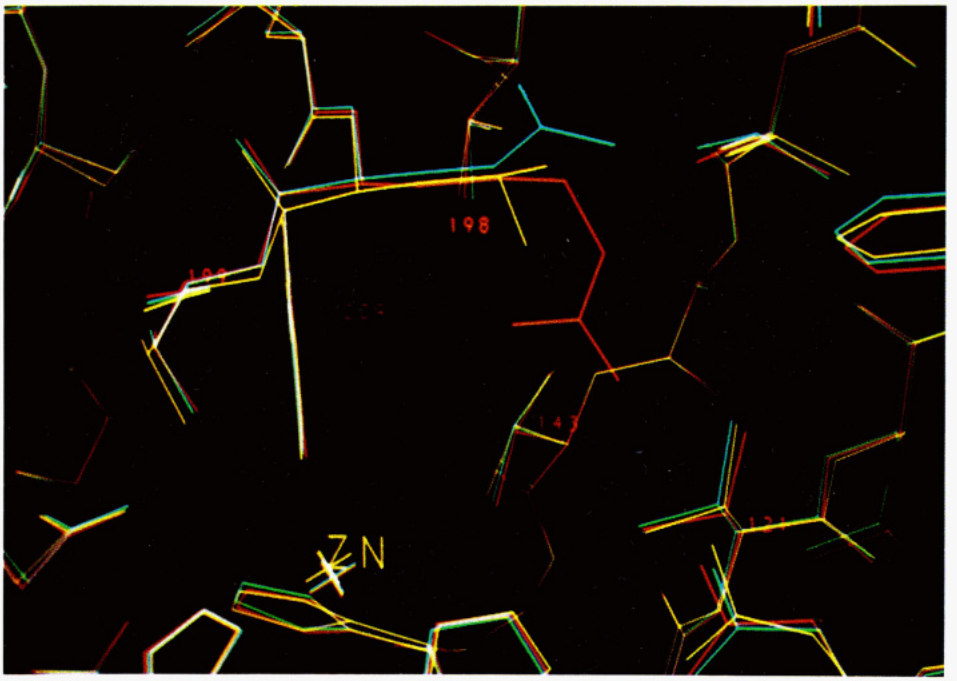

FIGURE 5: Least-squares superposition of the structures of wild-type CAII (yellow), L198E (cyan), and L198R (red). Enzyme residues Val-143, Thr-199, and the active site zinc are indicated; active site solvent molecules are omitted for clarity. Note the contrasting packing arrangements of the oppositely charged side chains. Additionally, there are no hydrogen bond contacts between the substituted side chains at residue 198 and the nonprotein zinc ligand.

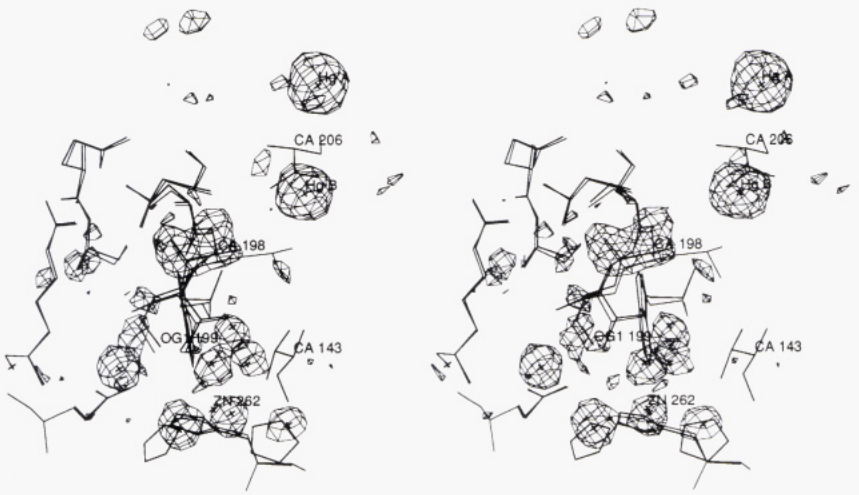

FIGURE 6: Difference electron density map of L198A CAII, calculated with Fourier coefficients ($|F_o| - |F_c|$) and phases calculated from the final model less the atoms of Ala-198, active site water molecules, and the two Hg^{2+} ions bound to residue Cys-206. The map is contoured at 2.5σ, and the refined atomic coordinates of L198A CAII are superimposed (thick bonds); residues Ala-198, Cys-206, and Hg^{2+} ions A and B are indicated. For comparison, the refined coordinates of wild-type CAII (thin bonds) are also superimposed. A small (ca. 0.45 Å) concerted movement of the loop containing residues 197–206 results from the accommodation of Hg^{2+} at site B.

of Arg-198 is 6.0 Å. Furthermore, the positively charged guanidinium group of Arg-198 makes no polar or van der Waals contact with the protein. Given the lack of bifurcated electron density corresponding to the guanidinium group, it is a reasonable suspicion that Arg-198 is somewhat mobile. Perhaps the mobility of this side chain results from a lack of hydrogen bond interactions with the rest of the protein. We note that this side chain undergoes a conformational change upon the binding of the inhibitor acetazolamide (Diamox) to the enzyme active site; moreover, Arg-198 is more clearly defined in electron density maps of the enzyme–inhibitor complex (Nair and Christianson, unpublished results). Therefore, comparable mobility of Arg-198 likely accommodates CO_2 association as the substrate approaches nucleophilic zinc-bound hydroxide.

The crystal structure of the remaining mutant, L198A CAII, reveals that the substitution of a smaller side chain at residue 198 widens the mouth of the hydrophobic pocket (an electron density map is found in Figure 6). There are no significant changes in the conformation of the polypeptide backbone in the region of Ala-198 (Table II). A superposition of wild-type and L198A CAIIs is found in Figure 6; the rms deviation of Cα atoms is 0.15 Å between the two structures. Interestingly, the Leu→Ala substitution allows for a well-ordered water molecule to hydrogen bond to the side chain of Thr-200, although this interaction does not exhibit optimal stereochemistry (Ippolito et al., 1990).

The cavity arising from the Leu→Ala substitution in L198A CAII additionally affects the metal binding properties of the enzyme. The mercury ion typically required for CAII

Table III: Zinc–Ligand Distances in CAII Variants (Å)

ligand	wild type	L198E	L198H	L198R	L198A
His-94	2.3	2.2	2.2	2.1	2.1
His-96	2.1	2.1	2.3	2.1	2.1
His-119	2.2	2.1	2.0	1.9	2.0
solvent	2.4	2.1	2.2	2.2	2.1

crystallization binds to Cys-206 at two sites in L198A CAII, designated A and B (Figure 6). This metal binding behavior contrasts with that observed for the wild-type and all other CAII variants, where only site A is occupied by Hg^{2+} (Eriksson et al., 1986, 1988; Alexander et al., 1991; Krebs et al., 1991; Nair et al., 1991). The bulky isobutyl side chain of Leu-198 sterically precludes the binding of Hg^{2+} to site B in the wild-type enzyme, but the substitution of a methyl group for this side chain in the L198A variant results in a small void that allows Hg^{2+} to bind to site B. The refined occupancies of $Hg^{2+}{}_A$ and $Hg^{2+}{}_B$ are 76% and 71%, respectively, indicating that mercury binding sites A and B are not mutually exclusive.

Although the L198A substitution affects mercury binding to Cys-206, no effect on zinc binding is evident in any Leu-198 variant of CAII. The protein ligands comprising the zinc coordination polyhedron of each variant do not undergo significant structural changes (Table III), even though the Cα of Leu-198 is only 6.7 Å from Zn^{2+}. Indeed, the closest contact between the side chain of a Leu-198 variant and zinc is 6.0 Å, and the closest contact between the side chain of a Leu-198 variant and a zinc ligand is 4.4 Å—this interaction is found in L198R CAII, and the contact occurs between the nonprotein zinc ligand and the NH1 group of Arg-198. We note that although the crystallizations of L198E and L198R CAIIs were performed in the presence of 3 mM NaN_3 [azide anion is a noncompetitive inhibitor; see Tibell et al. (1984) and Lindskog et al. (1991)], this concentration of azide does not generally perturb the protein or solvent structure of the enzyme (Nair & Christianson, 1993).

Finally, it should be noted that amino acid substitutions at Leu-198 do not appear to affect the conformational equilibrium of the catalytic proton shuttle, His-64 (Steiner et al., 1975; Tu et al., 1989). In L198E, L198H, L198R, and L198A CAIIs, this residue occupies the "in" conformation observed in the wild-type enzyme (Nair & Christianson, 1991). We note that the conformational equilibrium of His-64 can be altered by an amino acid substitution at Thr-200 (Krebs et al., 1991) and His-94 (Alexander et al., 1993), as well as the binding of sulfonamide inhibitors in the enzyme active site (Prugh et al., 1991; Baldwin et al., 1989; R. S. Alexander, A. Jain, G. M. Whitesides, and D. W. Christianson, unpublished results).

DISCUSSION

Role of the Hydrophobic Pocket. Spectroscopic (Bertini et al., 1979, 1983, 1987), computational (Merz, 1990, 1991; Liang & Lipscomb, 1990), and genetic–structure studies (Fierke et al., 1991; Alexander et al., 1991; Nair et al., 1991; Krebs et al., 1993; Nair and Christianson, present study) of various carbonic anhydrases are consistent with the role of the hydrophobic pocket as a precatalytic association site for substrate. Although the conservation of a well-defined pocket is critical for proper substrate association, catalysis is not severely compromised when the mouth of the pocket is widened. Parenthetically, we note that a deeper pocket does not significantly hinder efficient catalysis in Val-143→Gly CAII, but a shallower pocket in the Val-143→Tyr variant results in a 3×10^5-fold loss of CO_2 hydrase activity (Fierke et al., 1991; Alexander et al., 1991). The hydrophobic pocket is probably involved in desolvating the substrate as well as "funneling" the substrate toward nucleophilic zinc-bound hydroxide, and a wide variety of surface contours will satisfy this role—as long as minimal requirements of pocket width and depth are met. Surprisingly, the substitution of larger amino acids for Leu-198 does not severely violate the minimum width requirements, and the reasons for this are structural (e.g., the novel packing arrangements of Glu-198 in L198E CAII and His-198 in L198H CAII) or dynamic (e.g., the mobile side chain of Arg-198 in L198R CAII).

The superposition of CO_2 in a proposed enzyme–substrate complex (Merz, 1990, 1991) along with wild-type, L198H, and L198R CAIIs illustrates that the CO_2 association site is not sterically hindered by amino acid substitutions at Leu-198 (Figure 7). However, although the side chain of Arg-198 does not occupy the CO_2 association site, its predominant conformation would hinder access to this site. Therefore, the side chain of Arg-198 must be reasonably mobile to allow for CO_2 association, just as this side chain is sufficiently mobile to allow for inhibitor binding in the CAII active site (Nair and Christianson, unpublished results). Fourier transform infrared spectroscopic measurements on wild-type and L198R CAIIs indicate that the CAII–CO_2 dissociation constant increases 5-fold in the variant (Krebs et al., 1993), and this modest loss of enzyme–substrate affinity may reflect the energetic cost of the required conformational change of Arg-198.

The so-called deep water molecule, which is found at the mouth of the hydrophobic pocket, occupies the precatalytic association site for substrate CO_2 (Eriksson et al., 1986, 1988; Lindskog, 1986). Indeed, direct displacement of the deep water by the substitution of large, aromatic side chains at the base of the hydrophobic pocket in Val-143→Phe and Val-143→Tyr CAIIs results in severe catalytic losses of 5×10^4-fold and 3×10^5-fold, respectively (Fierke et al., 1991; Alexander et al., 1991). Amino acid substitutions which do not displace the deep water, as in Val-143→Gly and Val-121→Ala CAIIs, do not severely hinder catalysis (Fierke et al., 1991; Alexander et al., 1991; Nair et al., 1991); the same holds true for CAII variants at Leu-198 (Krebs et al., 1993). Therefore, a working hypothesis is that if the deep water is not displaced by amino acid substitutions in the hydrophobic pocket, then catalysis will not be severely compromised since CO_2 association will not be hindered.

Of course, subtle perturbations of individual steps in the catalytic mechanism may result from mutations that do not necessarily compromise the CO_2 association site. For example, subtle catalytic differences measured among Leu-198 variants may correspond to subtle changes in active site solvent structure found in each variant; in turn, changes in solvent structure may affect the kinetics of rate-limiting proton transfer. It is interesting that the most substantial catalytic losses are sustained when charged or larger amino acids are substituted for Leu-198, although these losses are not nearly as severe as those sustained for certain amino acid substitutions at Val-143 (Fierke et al., 1991; Alexander et al., 1991).

Given that an isotope effect on k_{cat} for CO_2 hydration is observed in all Leu-198 variants studied by Krebs et al. (1993), the intramolecular proton transfer between zinc-bound water and His-64 remains rate-limiting in these variants. Because of this, the effects of different Leu-198 variants on the trajectory of CO_2 association and desolvation in the CAII active site are difficult to establish solely by kinetic methods. However, Krebs et al. (1993) demonstrate that CAII–CO_2

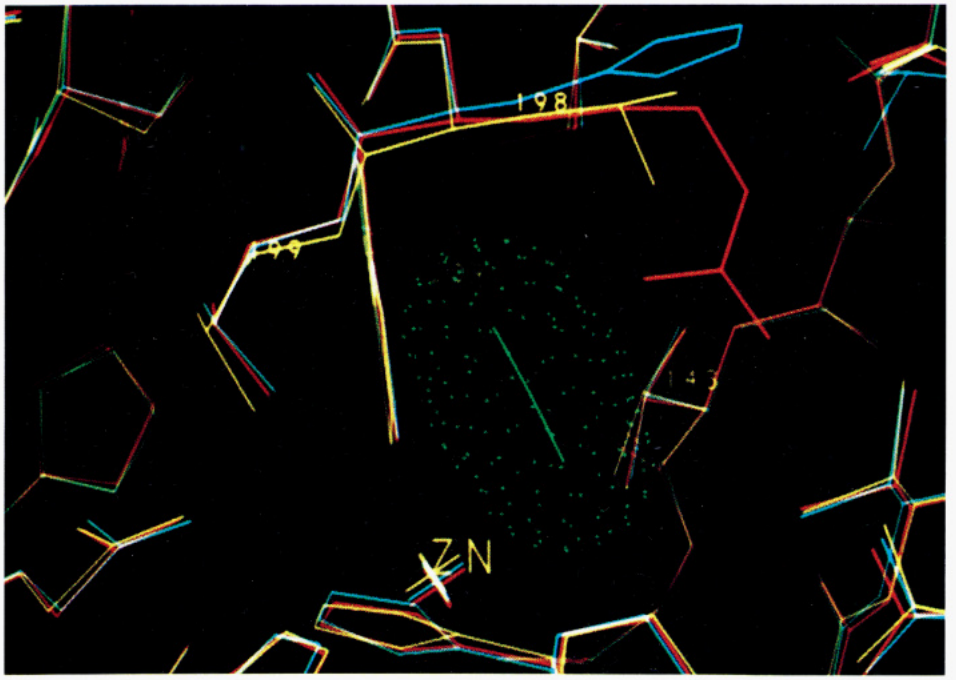

FIGURE 7: Coordinates of a proposed CO_2 binding mode (green, with van der Waals surface; Merz, 1990, 1991) superimposed on the structure of wild-type CAII (yellow), L198H (cyan), and L198R (red). Enzyme residues Val-143, Thr-199, and the active site zinc are indicated. Note that CO_2 association is not structurally hindered by the larger side chains in L198H and L198R CAIIs. However, the guanidinium side chain of Arg-198 must move in order to allow CO_2 unhindered access to the hydrophobic pocket.

association and affinity can be accurately evaluated by Fourier transform infrared spectroscopy, and differences in CO_2 affinity measured between wild-type and L198R CAIIs can be reconciled by structural differences observed in their respective hydrophobic pockets.

Residue 198 and Zinc-Bound Solvent. In general, the pK_a of zinc-bound solvent is not significantly altered in the CAII variants studied here [$\Delta pK_a \leq 1$; see Table II of Krebs et al. (1993)]. However, there is one notable exception: the pH dependence of L198E CAII-catalyzed esterase activity is parabolic, implicating functional groups with pK_a values of 5.9 and 8.9. This is suggestive of a mechanism in which esterase activity requires the ionization of another group in addition to zinc-bound solvent. Alternatively, it is a remote possibility that esterase activity does not require the ionization of zinc-bound solvent at all, but instead involves two additional functional groups.

Although $\Delta pK_a \leq 1$ in the Leu-198 variants studied, it is nonetheless interesting to note subtle ΔpK_a trends among these variants. For instance, the pK_a of zinc-bound solvent in L198H CAII is 7.9, and that of L198R CAII is 7.5; these values can be compared with the pK_a values of 6.9 measured for the wild-type enzyme (Krebs et al., 1993). These data are suggestive of counterion clustering about the polar or positively charged residue 198 side chain in each variant. For example, a dynamic cluster of sulfate anions (present in kinetic assay and crystallization media) could congregate around the Arg-198 side chain in the CAII active site, such that the zinc-bound solvent molecule could "feel" the electrostatic effect of the negatively charged counterion cluster (and not the positively charged side chain at the center of the cluster)—this would destabilize zinc-bound hydroxide such that an increased pK_a would result for zinc-bound solvent. These pK_a trends are opposite those that would be expected in the absence of counterion effects, and we suggest that these trends are similar to those observed to accompany ΔpK_a values for His-64 in certain subtilisin variants (Russell & Fersht, 1987).

Importantly, Leu-198 is not conserved between human carbonic anhydrase isozymes II (CAII) and III (CAIII)—in the latter isozyme, residue 198 is phenylalanine. It is suggested that the benzyl side chain of Phe-198 contributes to the relatively low CO_2 hydration activity of CAIII, for which $k_{cat}/K_M = 3 \times 10^5$ M^{-1} s^{-1}; indeed, the CAIII variant Phe-198→Leu exhibits enhanced CO_2 hydrase activity relative to the wild-type enzyme (LoGrasso et al., 1991, 1993). However, the converse situation does not apply: the Leu-198→Phe variant of CAII has a value of k_{cat}/K_M that is close to that measured for wild-type CAII and not CAIII (Lindskog et al., 1991).

The side-chain packing geometry of His-198 in L198H CAII provides a structural inference as to the packing of the Phe-198 side chain in Leu-198→Phe CAII. It is possible that the Leu→Phe substitution may actually result in a wider hydrophobic pocket, due to the packing of the Phe-198 side chain against the flanking hydrophobic wall. This would be consistent with the minimal functional ramifications of the Leu-198→Phe substitution (Lindskog et al., 1991). Furthermore, although noncovalent interactions between zinc-bound hydroxide and the side chain of Phe-198 are proposed to account for the diminished activity of CAIII (LoGrasso et al., 1991), there are no interactions between residue 198 side chains and the nonprotein ligand in any of the CAII structures reported herein. In L198H CAII, the closest contact between His-198 and zinc-bound hydroxide is 5.4 Å; the distance between the imidazole centroid of His-198 and zinc-bound hydroxide is 6.5 Å.

Finally, the structural results reported herein establish the prominence of CAII as an architectural paradigm for the engineering of specificity pockets in protein catalysts. To date, a total of nine CAII variants with engineered pockets have been structurally characterized by high-resolution X-ray crystallographic methods. These studies have illuminated the long-range structural changes which propagate through the protein structure in response to amino acid mutations at buried

or partially buried locations. The magnitude of a through-scaffolding, compensatory structural change is generally related to the solvent accessibility of the mutated side chain: mutations of core residues introduce larger structural changes in the protein scaffolding [e.g., see Alexander et al. (1991)] than alterations of surface side chains (Nair et al., 1991). Residues at the mouth of the hydrophobic pocket, such as Val-121 and Leu-198, are less buried than the residue at the base of the pocket (Val-143); consequently, smaller structural changes accompany mutations at these residues. However, a noticeable structural change is observed in L198A CAII, where the loop containing residues 197–206 endures a small (ca. 0.45 Å), concerted movement away from the active site. This compensatory structural change arises from Hg^{2+} binding at site B (Figure 6).

SUMMARY AND CONCLUSIONS

The hydrophobic pocket of CAII is critical for substrate association. However, efficient catalysis is relatively tolerant of amino acid substitutions at Leu-198, which is at the mouth of the hydrophobic pocket. At pH 8.9, the specific CO_2 hydrase activities of wild-type, L198E, L198H, L198R, and L198A CAII variants are 120, 6, 12, 7, and 35 μM^{-1} s^{-1}, respectively (Krebs et al., 1993). The three-dimensional structures of these variants provide a foundation for understanding the functional effects of hydrophobic → hydrophilic mutations in the pocket. Attempts to block the pocket by the substitution of larger side chains at position 198 do not severely hinder catalysis, since the minimum width of the pocket is maintained by side-chain packing or mobility.

It has been proposed that the so-called deep water, at the mouth of the hydrophobic pocket, must be displaced as substrate CO_2 approaches zinc-bound hydroxide (Eriksson et al., 1986, 1988; Lindskog, 1986). Amino acid substitutions which directly displace the deep water, e.g., Val-143→Tyr and Val-143→Phe, result in severely diminished activity (Fierke et al., 1991; Alexander et al., 1991). In contrast, significant activity is retained in enzyme variants where the displacement of the deep water is not a steric requirement (e.g., Val-143→Gly and Val-121→Ala CAIIs). Since mutations at Leu-198 do not displace the deep water, it is consistent that these substitutions do not severely hinder substrate association. Indeed, the direct measurement of enzyme–substrate dissociation constants by Fourier transform infrared spectroscopy reveals a 5-fold increase from wild-type CAII to L198R CAII (Krebs et al., 1993). In addition to differences in substrate association, subtle changes in active site solvent structure arising from Leu-198 substitutions may affect the kinetics of rate-limiting intramolecular proton transfer. However, subtle structure–activity relationships involving solvent are difficult to pinpoint at the resolution limit of these X-ray crystallographic structure determinations.

It should be noted that there are no close contacts between any of the substituted side chains at residue 198 and the nonprotein zinc ligand. Hence, the nucleophilicity of zinc–hydroxide is not directly affected by the hydrophobic → hydrophilic substitutions at residue 198 in most examples (Krebs et al., 1993). However, a larger ΔpK_a value for zinc-bound solvent is implicated by the pH dependence of ester hydrolysis by L198E CAII—here, the pK_a of zinc-bound water is perturbed to 8.9, and an additional enzyme-bound group of pK_a 5.9 (most likely the side chain of Glu-198) is implicated in the catalytic mechanism (Krebs et al., 1993). One possibility is that the water molecule hydrogen bonded to the carboxylate of Glu-198 participates in catalysis, thereby implicating Glu-198 as a general base. Future structural and functional studies of L198E CAII will delineate its novel catalytic features.

Finally, given the relatively minimal effects of the residue 198 side chain on the pK_a of zinc-bound solvent in CAII, it is instructive to compare these structure–function relationships with those observed in CAIII. Although close contacts between zinc-bound solvent and Phe-198 in *bovine* CAIII are proposed to account for diminished activity in that isozyme (LoGrasso et al., 1991, 1993), such contacts cannot predominate in Leu-198→Phe CAII, where normal activity measurements are reported (Lindskog et al., 1991). As acknowledged by these investigators, it is possible that activity differences between CAII and CAIII arise from more subtle structural differences between the two isozymes. Regarding the conformation of Phe-198 in Leu-198→Phe CAII, the aromatic side chain should pack against the flanking hydrophobic wall, well out of the way of zinc-bound hydroxide (e.g., in analogous fashion to the heteroaromatic side chain of His-198 in L198H CAII). The future X-ray crystallographic structure determination of Leu-198→Phe CAII may confirm this expectation.

ACKNOWLEDGMENT

We thank C. A. Fierke, J. F. Krebs, and J. A. Ippolito for helpful discussions.

REFERENCES

Alexander, R. S., Nair, S. K., & Christianson, D. W. (1991) *Biochemistry 30*, 11064–11072.

Alexander, R. S., Kiefer, L. L., Fierke, C. A., & Christianson, D. W. (1993) *Biochemistry 32*, 1510–1518.

Baldwin, J. J., Ponticello, G. S., Anderson, P. S., Christy, M. E., Murcko, M. A., Randall, W. C., Schwam, H., Sugrue, M. F., Springer, J. P., Grove, J., Mallorga, P., Viader, M.-P., McKeever, B. M., & Navia, M. A. (1989) *J. Med. Chem. 32*, 2510–2513.

Bernstein, F. C., Koetzle, T. F., Williams, G. J. B., Meyer, E. F., Brice, M. D., Rodgers, J. R., Kennard, O., Shimanouchi, T., & Tasumi, M. (1977) *J. Mol. Biol. 112*, 535–542.

Bertini, I., Borghi, E., & Luchinat, C. (1979) *J. Am. Chem. Soc. 101*, 7069–7071.

Bertini, I., Canti, G., Luchinat, C., & Borghi, E. (1983) *J. Inorg. Biochem. 18*, 221–229.

Bertini, I., Luchinat, C., Monnanni, R., Roelens, S., & Moratal, J. M. (1987) *J. Am. Chem. Soc. 109*, 7855–7856.

Bhat, T. N., Sasisekharan, V., & Vijayan, M. (1979) *Int. J. Pept. Protein Res. 13*, 170–184.

Christianson, D. W. (1991) *Adv. Protein Chem. 42*, 281–355.

Coleman, J. E. (1967) *J. Biol. Chem. 242*, 5212–5219.

Coleman, J. E. (1986) in *Zinc Enzymes* (Bertini, I., Luchinat, C., Maret, W., & Zeppezauer, M., Eds.) pp 49–58, Birkhauser, Boston, MA.

Durbin, R. M., Burns, R., Moulai, J., Metcalf, P., Freymann, D., Blum, M., Anderson, J. E., Harrison, S. C., & Wiley, D. C. (1986) *Science 232*, 1127–1132.

Eigen, M., & Hammes, G. G. (1963) *Adv. Enzymol. Relat. Subj. Biochem. 25*, 1–38.

Eriksson, A. E., Jones, T. A., & Liljas, A. (1986) in *Zinc Enzymes* (Bertini, I., Luchinat, C., Maret, W., & Zeppezauer, M., Eds.) pp 317–328, Birkhauser, Boston, MA.

Eriksson, A. E., Jones, T. A., & Liljas, A. (1988) *Proteins: Struct., Funct., Genet. 4*, 274–282.

Fierke, C. A., Calderone, T. L., & Krebs, J. F. (1991) *Biochemistry 30*, 11054–11063.

Hendrickson, W. A. (1985) *Methods Enzymol. 115*, 252–270.

Hendrickson, W. A., & Konnert, J. H. (1981) in *Biomolecular Structure, Conformation, Function and Evolution* (Srinivasan, R., Ed.) Vol. 1, pp 43–47, Pergamon, Oxford.

Ippolito, J. A., Alexander, R. S., & Christianson, D. W. (1990) *J. Mol. Biol. 215*, 457–471.
Janin, J., Wodak, S., Levitt, M., & Maigret, B. (1978) *J. Mol. Biol. 125*, 357–386.
Jones, T. A. (1985) *Methods Enzymol. 115*, 157–171.
Jonsson, B.-H., Steiner, H., & Lindskog, S. (1976) *FEBS Lett. 64*, 310–314.
Krebs, J. F., Fierke, C. A., Alexander, R. S., & Christianson, D. W. (1991) *Biochemistry 30*, 9153–9160.
Krebs, J. F., Rana, F., Dluhy, R. A., & Fierke, C. A. (1993) *Biochemistry* (preceding paper in this issue).
Liang, J.-Y., & Lipscomb, W. N. (1990) *Proc. Natl. Acad. Sci. U.S.A. 87*, 3675–3679.
Liljas, A., Kannan, K. K., Bergsten, P.-C., Waara, I., Fridborg, K., Strandberg, B., Carlbom, U., Jarup, L., Lovgren, S., & Petef, M. (1972) *Nature (London), New Biol. 235*, 131–137.
Lindskog, S. (1986) in *Zinc Enzymes* (Bertini, I., Luchinat, C., Maret, W., & Zeepezauer, M., Eds.) pp 307–316, Birkhauser, Boston, MA.
Lindskog, S., & Coleman, J. E. (1973) *Proc. Natl. Acad. Sci. U.S.A. 70*, 2505–2508.
Lindskog, S., Behravan, G., Engstrand, C., Forsman, C., Jonsson, B.-H., Liang, Z., Ren, X., & Xue, Y. (1991) in *Carbonic Anhydrase* (Botre, F., Gros, G., & Storey, B. T., Eds.) pp 1–13, VCH, Weinheim.
LoGrasso, P. V., Tu, C.-K., Jewell, D. A., Wynns, G. C., Laipis, P. J., & Silverman, D. N. (1991) *Biochemistry 30*, 8463–8470.
LoGrasso, P. V., Tu, C.-K., Chen, X., Taoka, S., Laipis, P. J., & Silverman, D. N. (1993) (submitted for publication).
Luzzati, P. V. (1952) *Acta Crystallogr. 5*, 802–810.
Merz, K. M. (1990) *J. Mol. Biol. 214*, 799–802.
Merz, K. M. (1991) *J. Am. Chem. Soc. 113*, 406–411.
Nair, S. K., & Christianson, D. W. (1991) *J. Am. Chem. Soc. 113*, 9455–9458.
Nair, S. K., & Christianson, D. W. (1993) *Eur. J. Biochem.* (in press).
Nair, S. K., Calderone, T. L., Christianson, D. W., & Fierke, C. A. (1991) *J. Biol. Chem. 266*, 17320–17325.
Ponder, J. W., & Richards, F. M. (1987) *J. Mol. Biol. 193*, 775–791.
Prugh, J. D., Hartman, G. D., Mallorga, P. J., McKeever, B. M., Michelson, S. R., Murcko, M. A., Schwam, H., Smith, R. L., Sondey, J. M., Springer, J. P., & Sugrue, M. F. (1991) *J. Med. Chem. 34*, 1805–1818.
Russell, A. J., & Fersht, A. R. (1987) *Nature 323*, 496–500.
Silverman, D. N., & Tu, C. K. (1975) *J. Am. Chem. Soc. 97*, 2263–2269.
Silverman, D. N., & Lindskog, S. (1988) *Acc. Chem. Res. 21*, 30–36.
Steigemann, W. (1974) Ph.D. Thesis, Max-Planck-Institut fur Biochemie, 8033 Martinsried bei Munchen, Germany.
Steiner, H., Jonsson, B.-H., & Lindskog, S. (1975) *Eur. J. Biochem. 59*, 253–259.
Tibell, L., Forsman, C., Simonsson, I., & Lindskog, S. (1984) *Biochim. Biophys. Acta 789*, 302–310.
Tu, C., Silverman, D. N., Forsman, C., Jonsson, B.-H., Lindskog, S. (1989) *Biochemistry 28*, 7913–7918.